η photoproduction on quasifree nucleons in the chiral quark model

Xian-Hui Zhong[1,*] and Qiang Zhao[2,3,†]

[1]*Department of Physics, Hunan Normal University, and Key Laboratory of Low-Dimensional Quantum Structures and Quantum Control of Ministry of Education, Changsha 410081, P. R. China*

[2]*Institute of High Energy Physics, Chinese Academy of Sciences, Beijing 100049, P. R. China*

[3]*Theoretical Physics Center for Science Facilities, Chinese Academy of Sciences, Beijing 100049, P. R. China*

(Received 10 June 2011; published 20 October 2011)

A chiral quark-model approach is adopted to study the η photoproduction off the quasifree neutron and proton from a deuteron target. Good descriptions of the differential cross sections, total cross sections, and beam asymmetries for these two processes are obtained in the low-energy region. For $\gamma p \to \eta p$, the dominant resonances are $S_{11}(1535)$, $S_{11}(1650)$, $D_{13}(1520)$, $D_{13}(1700)$, and $P_{13}(1720)$. For the $\gamma n \to \eta n$ process, the dominant resonances are $S_{11}(1535)$, $S_{11}(1650)$, $D_{13}(1520)$, $D_{15}(1675)$, and $P_{13}(1720)$. Furthermore, the u-channel backgrounds contribute significantly to the η photoproduction processes. The configuration mixings in $S_{11}(1535, 1650)$ and $D_{13}(1520, 1700)$ can be extracted (i.e., $\theta_S \simeq 26^\circ$ and $\theta_D \simeq 21^\circ$). It shows that the narrow bump-like structure around $W = 1.68$ GeV observed in $\gamma n \to \eta n$ can be naturally explained by the constructive interferences between $S_{11}(1535)$ and $S_{11}(1650)$. In contrast, the destructive interference between $S_{11}(1535)$ and $S_{11}(1650)$ produces the shallow dip around $W = 1.67$ GeV in $\gamma p \to \eta p$. The S-wave interfering behavior in the proton and neutron reactions is correlated with each other in the quark-model framework, and no new exotic nucleon resonances are needed in these two reactions. The helicity amplitudes of $S_{11}(1535)$, $S_{11}(1650)$, $D_{13}(1520)$, $D_{13}(1700)$, and $D_{15}(1675)$ are extracted from the reactions as well.

DOI: 10.1103/PhysRevC.84.045207 PACS number(s): 13.60.Le, 14.20.Gk, 12.39.Jh, 12.39.Fe

I. INTRODUCTION

The understanding the baryon spectrum and the search for the missing nucleon resonances and new exotic states are hot topics in nuclear physics [1]. The photoproduction of mesons is an ideal experimental tool for the study of nucleon resonances [2]. Recently, a bump structure around $W = 1.68$ GeV was observed in the excitation function of η production off quasifree neutrons by Ref. [3], which was considered as evidence for a narrow resonance. To further understand the "anomalous" peak around $W = 1.68$ GeV, the measurement of the polarized beam asymmetry in η photoproduction on the neutron was also carried out by the GRAAL Collaboration [4]. The bump-like structure observed in $\gamma n \to \eta n$ stimulates great interest from other experimental collaborations. The CBELSA/TAPS Collaboration measured the quasifree photoproduction of η mesons off nucleons bound in the deuteron [5] and found that there was a pronounced bump-like structure at $W \simeq 1.68$ GeV in the excitation function for η production off the neutron. This structure was absent in $\gamma p \to \eta p$. This structure was also confirmed in the η production off the neutron by the Laboratory of Nuclear Science (LNS), Tohoku University [6] and the Crystal Ball/TAPS Collaboration [7]. Very recently, the quasifree Compton scattering on the neutron was measured. The data reveals a narrow peak at $W \simeq 1.68$ GeV as well, which is considered as evidence for a narrow structure in the $\gamma n \to \eta n$ in association with the photoproduction data [8].

Explanations for the bump structure around $W \simeq 1.68$ GeV have been proposed in the literature. One proposal [9–13] is that the narrow structure might correspond to the antidecuplet of pentaquark states. The other possibility is that the narrow structure around $W \simeq 1.68$ GeV is due to the interferences of some well-known nucleon resonances. For example, Klempt *et al.* predict that the narrow structure can be naturally interpreted by interferences between $S_{11}(1535)$ and $S_{11}(1650)$ [14]. Similar conclusions are obtained by Shyam and Scholten within a coupled-channels K-matrix approach, where the the bump structure at $W \simeq 1.68$ GeV is attributed to the interfering effects of $S_{11}(1535)$, $S_{11}(1650)$, $P_{11}(1710)$, and $P_{13}(1710)$ [15]. In contrast, Shklyar *et al.* suggest that the narrow structure can be explained in terms of coupled-channel effects due to $S_{11}(1650)$ and $P_{11}(1710)$ resonance excitations [16].

It is also interesting to ask why the bump structure has not been observed in $\gamma p \to \eta p$ if it indeed corresponds to a genuine resonance. Kuznetsov *et al.* presented their new data of the beam asymmetry for η photoproduction on free protons, which may have revealed a structure [17]. However, it is questionable to explain this structure as evidence of a narrow resonance according to partial-wave analysis [14]. Very recently the MAMI-C Collaboration reported their new observations on $\gamma p \to \eta p$. A shallow dip near $W = 1.68$ GeV in the total cross section is found to be caused by a substantial dip in η production at forward angles [18]. It is wondered whether the dip structure is in connection with the observed narrow structure in the neutron reaction. To have a better understanding of these questions, a combined study of the η production off quasifree protons and neutrons is urgently needed.

*zhongxh@ihep.ac.cn
†zhaoq@ihep.ac.cn

In this work, we present a systemic analysis of experimental observables, such as differential cross sections, total cross sections, and polarized beam asymmetry, for the η photoproduction on the quasifree nucleons within a constituent quark model.

In the quark model, an effective chiral Lagrangian is introduced to account for the quark-pseudoscalar-meson coupling. Since the quark-meson coupling is invariant under the chiral transformation, some of the low-energy properties of QCD are retained. The chiral quark model has been well developed and widely applied to meson photoproduction reactions [19–31]. It has several obvious features. One is that only a limited number of parameters will appear in the formalism. In principle, only one parameter is needed for the resonances to be coupled to the pseudoscalar meson in the SU(6)⊗O(3) symmetric quark-model limit. This distinguishes it from hadronic models where each resonance requires one individual coupling constant as a free parameter. Second, all the resonances are treated equivalently at the quark level. Thus, it would have predictive powers to some extent when exposed to experimental data. Information about the resonance structures and form factors can thus be extracted. Meanwhile, insights into the SU(6)⊗O(3) symmetry breaking can be gained.

In the case of η meson photoproduction off nucleons, the chiral quark model can be applied and transition amplitudes at the tree level can be explicitly calculated. There are interesting differences between $\gamma p \to \eta p$ and $\gamma n \to \eta n$. In the γp reactions, contributions from states of representation $[70,^4 8]$ will be forbidden by the Moorhouse selection rule [32]. As a consequence, only states of $[56,^2 8]$ and $[70,^2 8]$ would contribute to the η production. In contrast, all the octet states can contribute to the γn reactions. In another word, more states will be present in the γn reactions. Therefore, by studying the η meson photoproduction on the quasifree nucleons, we expect that the role played by intermediate baryon resonances can be highlighted.

The paper is organized as follows: In Sec. II, a brief review of the chiral quark-model approach is given. The numerical results are presented and discussed in Sec. III. Finally, a summary is given in Sec. IV.

II. FRAMEWORK

In the chiral quark model, the quark-pseudoscalar-meson and electromagnetic (EM) couplings at the tree level are described by [22,24]

$$H_m = \sum_j \frac{1}{f_m} \bar{\psi}_j \gamma_\mu^j \gamma_5^j \psi_j \vec{\tau} \cdot \partial^\mu \vec{\phi}_m, \tag{1}$$

$$H_e = -\sum_j e_j \gamma_\mu^j A^\mu(\mathbf{k}, \mathbf{r}), \tag{2}$$

where ψ_j represents the jth quark field in a hadron and f_m is the meson's decay constant. The pseudoscalar-meson octet ϕ_m is written as

$$\phi_m = \begin{pmatrix} \frac{1}{\sqrt{2}}\pi^0 + \frac{1}{\sqrt{6}}\eta & \pi^+ & K^+ \\ \pi^- & -\frac{1}{\sqrt{2}}\pi^0 + \frac{1}{\sqrt{6}}\eta & K^0 \\ K^- & \bar{K}^0 & -\sqrt{\frac{2}{3}}\eta \end{pmatrix}. \tag{3}$$

The s- and u-channel transition amplitudes are determined by

$$\mathcal{M}_s = \sum_j \langle N_f | H_m | N_j \rangle \langle N_j | \frac{1}{E_i + \omega_\gamma - E_j} H_e | N_i \rangle, \tag{4}$$

$$\mathcal{M}_u = \sum_j \langle N_f | H_e \frac{1}{E_i - \omega_m - E_j} | N_j \rangle \langle N_j | H_m | N_i \rangle, \tag{5}$$

where ω_γ is the energy of the incoming photons. $|N_i\rangle$, $|N_j\rangle$, and $|N_f\rangle$ stand for the initial, intermediate, and final states, respectively, and their corresponding energies are E_i, E_j, and E_f, which are the eigenvalues of the nonrelativistic constituent quark model (NRCQM) Hamiltonian $\hat{H}$ [33,34]. The s- and u-channel transition amplitudes have been worked out in the harmonic oscillator basis in Ref. [22]. The t-channel contributions due to vector meson exchange are not considered in this work. If a complete set of resonances are included in the s and u channels, the introduction of t-channel contributions might result in double counting [35]. In fact, the t-channel vector-meson exchange contribution was found to be negligible in the low-energy region [24,36].

In the Chew-Goldberger-Low-Nambu (CGLN) parameterization [37], the transition amplitude can be written with a standard form:

$$\mathcal{M} = i f_1 \boldsymbol{\sigma} \cdot \boldsymbol{\epsilon} + f_2 \frac{(\boldsymbol{\sigma} \cdot \mathbf{q})\boldsymbol{\sigma} \cdot (\mathbf{k} \times \boldsymbol{\epsilon})}{|\mathbf{q}||\mathbf{k}|} + i f_3 \frac{(\boldsymbol{\sigma} \cdot \mathbf{k})(\mathbf{q} \cdot \boldsymbol{\epsilon})}{|\mathbf{q}||\mathbf{k}|} + i f_4 \frac{(\boldsymbol{\sigma} \cdot \mathbf{q})(\mathbf{q} \cdot \boldsymbol{\epsilon})}{|\mathbf{q}|^2}, \tag{6}$$

where $\boldsymbol{\sigma}$ is the spin operator of the nucleon, $\boldsymbol{\epsilon}$ is the polarization vector of the photon, and $\mathbf{k}$ and $\mathbf{q}$ are incoming photon and outgoing meson momenta, respectively.

It is should be remarked that the amplitudes in terms of the harmonic oscillator principle quantum number n are the sum of a set of SU(6) multiplets with the same n. To see the contributions of individual resonances, we need to separate out the single-resonance-excitation amplitudes within each principle number n in the s channel. Taking into account the width effects of the resonances, the resonance transition amplitudes of the s channel can be generally expressed as [22]

$$\mathcal{M}_R^s = \frac{2M_R}{s - M_R^2 + i M_R \Gamma_R(\mathbf{q})} \mathcal{O}_R e^{-(\mathbf{k}^2 + \mathbf{q}^2)/6\alpha^2}, \tag{7}$$

where $\sqrt{s} = E_i + \omega_\gamma$ is the total energy of the system, α is the harmonic oscillator strength, M_R is the mass of the s-channel resonance with a width $\Gamma_R(\mathbf{q})$, and $\mathcal{O}_R$ is the separated operators for individual resonances in the s channel. Its general structure is given by [22]

$$\mathcal{O}_R = g_R A \big[f_1^R \boldsymbol{\sigma} \cdot \boldsymbol{\epsilon} + i f_2^R (\boldsymbol{\sigma} \cdot \mathbf{q})\boldsymbol{\sigma} \cdot (\mathbf{k} \times \boldsymbol{\epsilon}) + f_3^R (\boldsymbol{\sigma} \cdot \mathbf{k})(\mathbf{q} \cdot \boldsymbol{\epsilon}) + f_4^R (\boldsymbol{\sigma} \cdot \mathbf{q})(\mathbf{q} \cdot \boldsymbol{\epsilon}) \big], \tag{8}$$

where g_R is an isospin factor, A is the meson decay amplitude, and f_i^R $(i = 1, 2, 3, 4)$ is proportional to the photon transition amplitude. The detail of extracting $\mathcal{O}_R$ can be found in Ref. [22].

Finally, the physical observables, differential cross section, and photon beam asymmetry are given by the following standard expressions [38]:

$$\frac{d\sigma}{d\Omega} = \frac{\alpha_e \alpha_m (E_i + M_N)(E_f + M_N)}{16 s M_N^2} \frac{1}{2} \frac{|\mathbf{q}|}{|\mathbf{k}|} \sum_i^4 |H_i|^2, \quad (9)$$

$$\Sigma = \frac{2\mathrm{Re}(H_4^* H_1 - H_3^* H_2)}{\sum_i^4 |H_i|^2}, \quad (10)$$

where α_m is the meson-nucleon-nucleon coupling constant and α_e is the fine-structure constant. The helicity amplitudes H_i can be expressed by the CGLN amplitudes f_i with the relations [38]

$$H_1 = -\frac{1}{\sqrt{2}} \sin\theta \cos\frac{\theta}{2}(f_3 + f_4), \quad (11)$$

$$H_2 = \sqrt{2} \cos\frac{\theta}{2}\left[(f_2 - f_1) + \sin^2\frac{\theta}{2}(f_3 - f_4)\right], \quad (12)$$

$$H_3 = \frac{1}{\sqrt{2}} \sin\theta \sin\frac{\theta}{2}(f_3 - f_4), \quad (13)$$

$$H_4 = \sqrt{2} \sin\frac{\theta}{2}\left[(f_2 + f_1) + \cos^2\frac{\theta}{2}(f_3 - f_4)\right]. \quad (14)$$

In this work, we study the η mesons' photoproduction off quasifree proton and neutron from a deuteron target. The deuteron is at rest in the laboratory system, but the nucleons are not. Thus, the Fermi motion of the quasifree nucleon should be included. To take into account the Fermi motion, we follow the method of Ref. [14] and fold the cross section for the free nucleon case with the momentum distribution of the nucleon inside the deuteron. This method is also adopted in Ref. [39].

The quasifree nucleon bound in the deuteron has a internal Fermi momentum $\mathbf{p}_N$. Its three components are defined as

$$\begin{aligned} p_{xN} &= |\mathbf{p}_N| \sin\Theta_N \cos\phi_N, \\ p_{yN} &= |\mathbf{p}_N| \sin\Theta_N \sin\phi_N, \quad p_{zN} = |\mathbf{p}_N| z_N. \end{aligned} \quad (15)$$

The outgoing meson momentum $\mathbf{q}$ has a relation with the internal Fermi momentum $\mathbf{p}_N$ [14]:

$$|\mathbf{q}| = \frac{\Sigma\xi|\mathbf{P}^m| + P_0^m\sqrt{\Sigma^2 - m_1^2\left[\left(P_0^m\right)^2 - |\mathbf{P}^m|^2\xi\right]}}{\left(P_0^m\right)^2 - |\mathbf{P}^m|^2\xi}, \quad (16)$$

where we have defined

$$\Sigma = \frac{1}{2}\left(s_{\mathrm{tot}} - m_1^2 - M_N^2\right), \quad (17)$$

$$\xi = \frac{z P_z^m + |\mathbf{p}_N|\sqrt{1 - z_N^2}\sqrt{1 - z^2}\cos\phi_N}{|\mathbf{P}^m|}, \quad (18)$$

$$|\mathbf{P}^m| = \frac{M_N(p_{zN} + \omega_\gamma) - \omega_\gamma(p_{0N} - p_{zN})}{\sqrt{s_{\mathrm{eff}}}} + \omega_\gamma, \quad (19)$$

$$P_0^m = \frac{M_N(p_{0N} + \omega_\gamma) + \omega_\gamma(p_{0N} - p_{zN})}{\sqrt{s_{\mathrm{eff}}}}. \quad (20)$$

In the above equations, z is the cosine of the angle between meson and photon (i.e., $z \equiv \cos\theta$), m_1 is the mass of the outgoing meson, and the several variables are defined as

$$p_{0N} = \sqrt{M_N^2 + |\mathbf{p}_N|^2}, \quad (21)$$

$$s_{\mathrm{tot}} = M_N^2 + 2\omega_\gamma(p_{0N} - |\mathbf{p}_N| z_N), \quad (22)$$

$$\sqrt{s_{\mathrm{eff}}} = \sqrt{M_N^2 + 2M_N\omega_\gamma}, \quad (23)$$

$$P_z^m = \frac{M_N p_{0N} + \omega_\gamma(p_{0N} - p_{zN} + M_N)}{\sqrt{s_{\mathrm{eff}}}} - \frac{\sqrt{s_{\mathrm{eff}}}}{M_N}(p_{0N} - p_{zN}). \quad (24)$$

Thus, the differential cross section for the meson photoproduction off nucleons bound in a deuteron can be expressed as [14]

$$\frac{d\sigma_{\gamma D}}{d\Omega} = \int \frac{d\sigma}{d\Omega} f^2(\mathbf{p}_N)|\mathbf{p}_N|^2 d|\mathbf{p}_N| \frac{dz_N d\phi_N}{4\pi}, \quad (25)$$

where $f^2(\mathbf{p}_N)$ is the nucleon momentum distribution inside the deuteron. In the calculations, we can choose the simple parametrization of the Paris [40] or CD-Bonn deuteron functions [41]. Both of the parametrizations give nearly the same wave functions for deuteron.

III. CALCULATIONS AND ANALYSIS

A. Parameters

In our framework, the resonance transition operator $\mathcal{O}_R$ is derived in the SU(6)⊗O(3) symmetric quark-model limit. In reality, the SU(6)⊗O(3) symmetry is generally broken due to, for example, spin-dependent forces in the quark-quark interaction. As a consequence, configuration mixings would occur, and an analytic solution cannot be achieved. An empirical way [28–31] to accommodate the configuration mixings in the symmetric quark model framework is to introduce a set of coupling-strength parameters C_R for each resonance amplitude,

$$\mathcal{O}_R \to C_R \mathcal{O}_R, \quad (26)$$

where C_R can be determined by fitting the experimental observables. In the SU(6)⊗O(3) symmetry limit, one finds $C_R = 1$ while deviations of C_R from unity imply SU(6)⊗O(3) symmetry breaking. For those two S-wave $1/2^-$ and D-wave $3/2^-$ states, state mixings seem to be inevitable. We explicitly express the transition amplitudes as follows:

$$\mathcal{O}_R \to C_R^{[70,^2 8]} \mathcal{O}_{[70,^2 8,J]} + C_R^{[70,^4 8]} \mathcal{O}_{[70,^4 8,J]}, \quad (27)$$

where the coefficients $C_R^{[70,^2 8]}$ and $C_R^{[70,^4 8]}$ should contain state-mixing information and from which the mixing angles between $S_{11}(1535)$ and $S_{11}(1650)$ and $D_{13}(1520)$ and $D_{13}(1700)$ can be extracted. The determined C_R values for low-lying resonances are listed in Table I, which are in agreement with the previous quark-model study of Ref. [29]. We will discuss them in detail in the later subsections.

To take into account the relativistic effects [21], the commonly applied Lorentz boost factor is introduced in the

TABLE I. Strength parameters C_R determined by experimental data.

Parameter	$\gamma n \to \eta n$	$\gamma p \to \eta p$	$\gamma p \to \eta p$ [29]
$C^{[70,^2 8]}_{S_{11}(1535)}$	0.85	1.10	1.120
$C^{[70,^4 8]}_{S_{11}(1535)}$	1.66		
$C^{[70,^2 8]}_{S_{11}(1650)}$	−0.14	−0.22	−0.200
$C^{[70,^4 8]}_{S_{11}(1650)}$	1.29		
$C^{[70,^2 8]}_{D_{13}(1520)}$	1.21	1.80	0.964
$C^{[70,^4 8]}_{D_{13}(1520)}$	0.78		
$C^{[70,^2 8]}_{D_{13}(1700)}$	0.34	0.50	0.036
$C^{[70,^4 8]}_{D_{13}(1700)}$	1.90		
$C_{D_{15}(1675)}$	1.80		
$C_{P_{13}(1720)}$	3.00	0.81	1.000
$C_{P_{13}(1900)}$	−1.00	−1.00	−2.478

resonance amplitude for the spatial integrals, which is

$$\mathcal{O}_R(\mathbf{k}, \mathbf{q}) \to \mathcal{O}_R(\gamma_k \mathbf{k}, \gamma_q \mathbf{q}), \tag{28}$$

where $\gamma_k = M_N/E_i$ and $\gamma_q = M_N/E_f$.

The ηNN coupling α_η is a free parameter in the present calculations and will be determined by the experimental data. In the present work the overall parameter ηNN coupling α_η is set to be the same for both the processes $\gamma n \to \eta n$ and $\gamma p \to \eta p$. Our ηNN coupling thus determined, $g_{\eta NN} \simeq 2.13$ [i.e., $\alpha_\eta \equiv g^2_{\eta NN}/(4\pi) = 0.36$], is in good agreement with the determinations in Refs. [27,42–44].

There are another two overall parameters, the constituent quark mass m_q and the harmonic oscillator strength α, from the transition amplitudes. In the calculation we adopt their standard values in the the quark model: $m_q = 330$ MeV and $\alpha^2 = 0.16$ GeV^2.

In the calculations, we allow the resonance masses and widths to have some changes around the values from the particle data group (PDG) to better describe the data. The determined values are listed in Table II. It is found that most of the resonance masses and widths are in the range of PDG values. The favorable widths of $S_{11}(1535)$ and $S_{11}(1650)$ are 119 MeV and 105 MeV, respectively, which are slightly smaller than the lower limit of the PDG values [45].

TABLE II. Breit-Wigner masses M_R (MeV) and widths Γ_R (MeV) for the resonances in the s channel.

Resonance	M_R	Γ_R	M_R (PDG)	Γ_R (PDG)
$S_{11}(1535)$	1520	119	1535 ± 10	150 ± 25
$S_{11}(1650)$	1630	105	1655^{+15}_{-10}	165 ± 20
$D_{13}(1520)$	1525	100	1520 ± 5	115^{+10}_{-15}
$D_{13}(1700)$	1690	110	1700 ± 50	100 ± 50
$D_{15}(1675)$	1675	140	1675 ± 5	150^{+15}_{-20}
$P_{13}(1720)$	1700	167	1720^{+30}_{-20}	200^{+100}_{-50}

B. $\gamma p \to \eta p$ with free proton target

The chiral quark-model studies of $\gamma p \to \eta p$ have been carried out in Refs. [25,27–31]. The improvement of the experimental situations allows one to determine the free parameters introduced in the formulation. In this channel the N^* states of representation $[70,^4 8]$ are prohibited from contribution because of the Moorhouse selection rule [32]. This would significantly reduce the number of s-channel resonances in the reaction in the SU(6)⊗O(3) symmetry limit. However, the configuration mixing effects would violate this selection rule, and mixings between representations of $[70,^2 8]$ and $[70,^4 8]$ with the same quantum numbers have to be taken into account in order to obtain a good description of the data near threshold.

To be more specific, $S_{11}(1535)$ and $S_{11}(1650)$ as mixing states of $|70,^2 8, 1/2^-\rangle$ and $|70,^4 8, 1/2^-\rangle$ can be expressed as follows:

$$\begin{aligned} S_{11}(1535) &= \cos\theta_S |70,^2 8, 1/2^-\rangle - \sin\theta_S |70,^4 8, 1/2^-\rangle, \\ S_{11}(1650) &= \sin\theta_S |70,^2 8, 1/2^-\rangle + \cos\theta_S |70,^4 8, 1/2^-\rangle, \end{aligned} \tag{29}$$

where θ_S is the mixing angle. Taking into account that the strong transition ratio $R^N_S \equiv \langle N|H_m|70,^4 8, 1/2^-\rangle/\langle N|H_m|70,^2 8, 1/2^-\rangle = -1$, and that the EM transition amplitude $\langle p|H_e|70,^4 8\rangle = 0$ in the symmetric quark model due to the Moorhouse selection rule [32], the $S_{11}(1535)$ and $S_{11}(1650)$ transition amplitudes will only involve the term of $[70,^2 8]$ representations defined in Eq. (27), of which the coefficients can be expressed as follows:

$$\begin{aligned} C^{[70,^2 8]}_{S_{11}(1535)} &= \cos\theta_S\big(\cos\theta_S - R^N_S \sin\theta_S\big), \\ C^{[70,^2 8]}_{S_{11}(1650)} &= \sin\theta_S\big(\sin\theta_S + R^N_S \cos\theta_S\big). \end{aligned} \tag{30}$$

By fitting the data for $\gamma p \to \eta p$ to determine the above coefficients and taking their ratio, one can extract the mixing angle θ_S. In particular, it shows that the data favor $C^{[70,^2 8]}_{S_{11}(1535)} \simeq 1.10$ and $C^{[70,^2 8]}_{S_{11}(1650)} \simeq -0.22$, which are compatible with the previous quark-model determinations [29–31]. These values lead to a mixing angle $\theta_S \simeq 24^\circ \sim 32^\circ$, which is consistent with the mixing angles determined by the partial decay widths of $S_{11}(1535)$ and $S_{11}(1650) \to \pi N$ and ηN recently [48]. In Refs. [29,49], the relation of Eq. (30) was also obtained. However, the extracted mixing angle $\theta_S = -35^\circ \sim -27^\circ$ appears to have a sign difference from ours. This question has been clarified in their recent work [50]. In Refs. [29–31,49], the old conventions of the SU(3) wave functions from Isgur and Karl's early works [33,34] were adopted, which resulted in $R^N_S = 1$. Thus, a negative value for the mixing angle θ_S was obtained. We suggest the adoption of Isgur's later conventions of the SU(3) wave functions [51] in the studies, with which the relative signs among the resonances transition amplitudes can be avoided. In line with the Isgur's later conventions, $R^N_S = -1$ can be determined such that a positive value for the mixing angle θ_S can be extracted.

Equation (30) provides a rather general relation for the $[70,^2 8, 1/2^-]$ and $[70,^2 8, 1/2^-]$ mixings in $\gamma p \to \eta p$. It has

also an interesting implication of the mixing-angle range in terms of the experimental observations. Since the experimental data so far suggest the dominance of $S_{11}(1535)$ near threshold, the absolute value of $|C^{[70,^2 8]}_{S_{11}(1535)}/C^{[70,^2 8]}_{S_{11}(1650)}| \gg 1$. It should be noted that the positive mixing angle θ_S is consistent with the one-pion exchange (OPE) models [52], $1/N_c$ expansion approach [53], and the $^3P_0$ pair creation model [54]. The one-gluon exchange (OGE) model gives a negative value for the mixing angle which is also natural since in the OGE model the interacting vertex is defined differently [33].

Similarly, $D_{13}(1520)$ and $D_{13}(1700)$ as mixing states of $|70,^2 8, \frac{3}{2}^-\rangle$ and $|70,^4 8, \frac{3}{2}^-\rangle$ are expressed as follows:

$$\begin{aligned} D_{13}(1520) &= \cos\theta_D|70,^2 8, 3/2^-\rangle - \sin\theta_D|70,^4 8, 3/2^-\rangle, \\ D_{13}(1700) &= \sin\theta_D|70,^2 8, 3/2^-\rangle + \cos\theta_D|70,^4 8, 3/2^-\rangle, \end{aligned} \tag{31}$$

where θ_D is the mixing angle. The configuration mixing coefficient can be extracted as follows:

$$\begin{aligned} C^{[70,^2 8]}_{D_{13}(1520)} &= R\cos\theta_D(\cos\theta_D - \sin\theta_D/\sqrt{10}), \\ C^{[70,^2 8]}_{D_{13}(1700)} &= R\sin\theta_D(\sin\theta_D + \cos\theta_D/\sqrt{10}), \end{aligned} \tag{32}$$

where the factor $1/\sqrt{10}$ is given by $R^N_D \equiv \langle N|H_m|70,^4 8, 3/2^-\rangle/\langle N|H_m|70,^2 8, 3/2^-\rangle = 1/\sqrt{10}$ in the η production. The parameter R is introduced to adjust the overall D-wave strength. In $\gamma p \to \eta p$ due to the absence of the $\langle p|H_e|70,^4 8\rangle = 0$ helicity amplitude at leading order, the amplitude of $\langle p|H_e|70,^2 8\rangle$ cannot be well constrained. This amplitude will be canceled out when taking the ratio of these two D-wave excitation amplitudes. The deviation of R from unity may imply the underestimate of the EM transition amplitudes $\langle p|H_e|70,^2 8\rangle$ in the symmetric quark model. In fact, it shows that the $D_{13}(1520)$ helicity coupling $A^p_{3/2} \simeq 0.095$ GeV$^{-1/2}$ is underestimated by about a factor of 1.8 compared with the PDG value [45]. In $\gamma p \to \eta p$, the data favor $C_{D_{13}(1520)} \simeq 1.80$ and $C_{D_{13}(1700)} \simeq 0.50$, which leads to a mixing angle $\theta_D \simeq 21^\circ$ and $R \simeq 2.4$. The extracted mixing angle is comparable with that extracted from the OPE models [52], the $1/N_c$ expansion approach [53], the $^3P_0$ pair-creation model [54], and the chiral constituent quark approach [55].

In Figs. 1, 2, and 3, we plot the differential cross sections, fixed-angle excitation functions, and total cross section for $\gamma p \to \eta p$, respectively. These observables can be well described with the parameters determined by fitting 560 data points of the differential cross sections from Ref. [18] in the energy region 0.748 GeV $\leqslant E_\gamma \leqslant$ 1.3 GeV. The χ^2 per datum point is about $\chi^2/N = 2.9$. The dominant low-lying resonances are $S_{11}(1535)$, $S_{11}(1650)$, $D_{13}(1520)$, $D_{13}(1700)$, and $P_{13}(1720)$. In Table III we can see that the value of χ^2/N increases drastically if we switch off any one of those resonances. This is to show a reasonable control of the model parameters near threshold. The well-determined amplitudes are then applied to the quasifree reaction with the deuteron target.

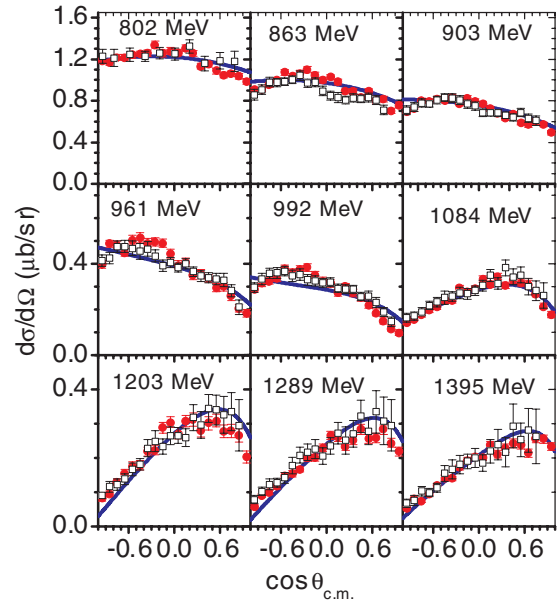

FIG. 1. (Color online) Differential cross sections for the η photoproduction off free proton at various beam energies. The data are taken from Refs. [18] (circles) and [46] (squares).

C. $\gamma p \to \eta p$ with quasifree proton target

Taking into account the Fermi motion, our predictions for the differential cross sections for the η photoproduction off the quasifree proton are shown in Fig. 4. It shows that the predictions are in a good agreement with the data from threshold to $E_\gamma \simeq 1.4$ GeV. In this energy region, the $S_{11}(1535)$ dominates the reaction, and the $D_{13}(1520)$ is crucial for accounting for the shape deviation from the S wave. The u

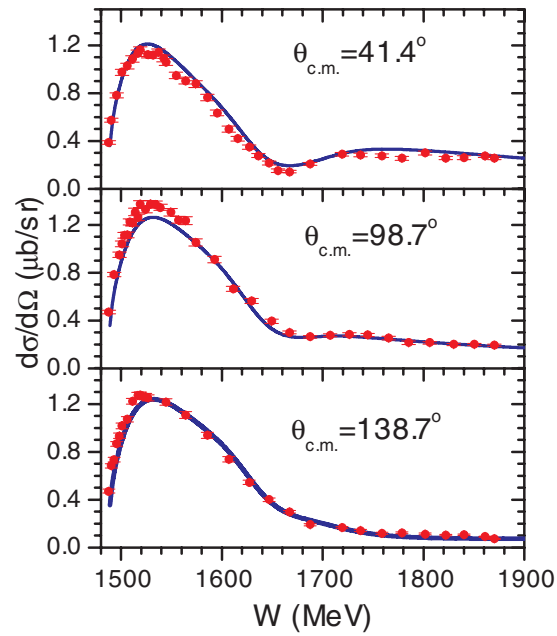

FIG. 2. (Color online) Fixed-angle excitation functions as a function of center-of-mass (c.m.) energy W for the η photoproduction off free proton. The circles stand for the data from Ref. [18].

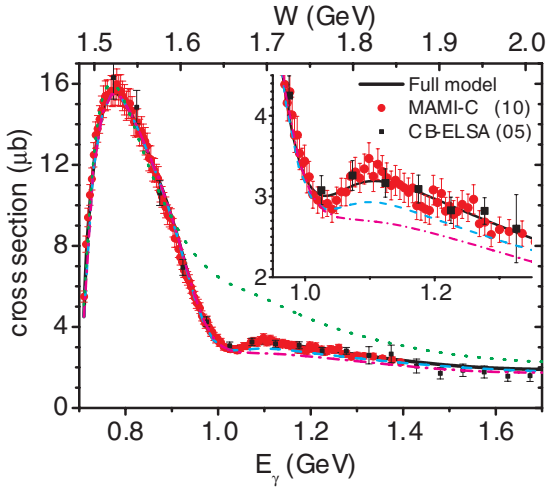

FIG. 3. (Color online) Total cross section for the η photoproduction off the free proton. The circles and squares stand for the data from Refs. [18] and [47], respectively. The dotted, dashed, and dash-dotted curves are for the results by switching off the contributions from $S_{11}(1650)$, $P_{13}(1720)$, and $D_{13}(1700)$, respectively.

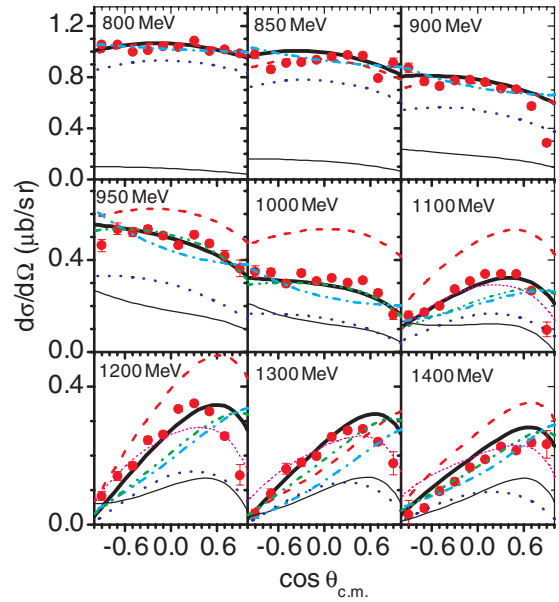

FIG. 4. (Color online) Differential cross sections for the η photoproduction off the quasifree proton at various beam energies. The data are taken from Ref. [5]. The solid curves correspond to the full-model result. The thin solid, dashed, dash-dotted, dash-dot-dotted, short dashed, and dotted curves are for the results by switching off the contributions from $S_{11}(1535)$, $S_{11}(1650)$, $D_{13}(1520)$, $D_{13}(1700)$, $P_{13}(1720)$, and the u channel, respectively.

channel also affects the differential cross section. By switching off the amplitudes of $S_{11}(1535)$ (thin solid curves), $D_{13}(1520)$ (dash-dotted curves), or the u channel (dotted curves), we see that the differential cross sections change drastically.

Similar to the free nucleon reaction, the state mixings between $[70,^2 8]$ and $[70,^4 8]$ are important. For $S_{11}(1535)$ and $S_{11}(1650)$, their mixing angle is fixed in the free nucleon reaction. In this sense, the quasifree reaction can be treated as a test of the mixing scenario near threshold. The relative destructive interference between $S_{11}(1535)$ and $S_{11}(1650)$ accounts for the sudden change of the angular distributions around $E_\gamma = 1.00$ GeV. In this energy region, the dashed curves indicate that without the contributions of $S_{11}(1650)$ the differential cross sections would be enhanced significantly. It should be mentioned that the destructive interference between $S_{11}(1535)$ and $S_{11}(1650)$ also accounts for the dip structure around $W = 1670$ MeV in the $\gamma p \to \eta p$ excitation function at forward angles recently observed by the MAMI-C Collaboration (see Fig. 2).

It can be also recognized that $D_{13}(1700)$ plays an important role around $E_\gamma = (1.0 \sim 1.1)$ GeV. We find that a sizable strength of $D_{13}(1700)$ (i.e., $C_{D_{13}(1700)} = 0.50$), is needed in order to account for the angular distributions. According to our analysis, $D_{13}(1700)$ is the main contributor to the bump structure around $W = 1.7$ GeV recently observed by the MAMI-C Collaboration in the cross section of the η production off free proton (see Fig. 3). It should be pointed out that, in the present work, we include sizable contributions from $D_{13}(1700)$ to improve the agreement with the data for the differential cross sections, which is compatible with the suggestion of Nakayama *et al.* [56]. Another possible explanation was discussed within the quark model [28–31], where a new S_{11} with a mass of $\sim$1.72 GeV was suggested to be included to improve the descriptions of the differential cross sections.

The P-wave state $P_{13}(1720)$ turns out to have rather small effects on the cross section near threshold, but shows up in the region of $E_\gamma = 1.2 \sim 1.4$ GeV in the forward angle direction shown by the short dashed lines. Some contributions of $P_{13}(1720)$ in the $\gamma p \to \eta p$ reaction were also suggested in Refs. [15,30,56].

The u channel plays an important role in the reactions. The dotted curves show that by turning off the contributions of u-channel backgrounds, the cross sections will be underestimated significantly.

In Fig. 5, the total cross section and the exclusive cross sections of several single resonances are shown. Our results are in good agreement with the data up to $E_\gamma \simeq 1.8$ GeV. The thin line in the upper panel of Fig. 5 denotes the result

TABLE III. χ^2 per datum point for the $\gamma p \to \eta p$ (free) and $\gamma n \to \eta n$ (quasifree). To quantify the role played by different resonances, the values after removing the corresponding resonances are also listed.

	Full Model	$S_{11}(1535)$	$S_{11}(1650)$	$D_{13}(1520)$	$D_{13}(1700)$	$D_{15}(1675)$	$P_{13}(1720)$
χ^2/N $(\gamma p \to \eta p)$	2.9	240	73.8	7.3	4.4		4.1
χ^2/N $(\gamma n \to \eta n)$	1.6	120	5.1	2.3	1.6	3.3	4.0

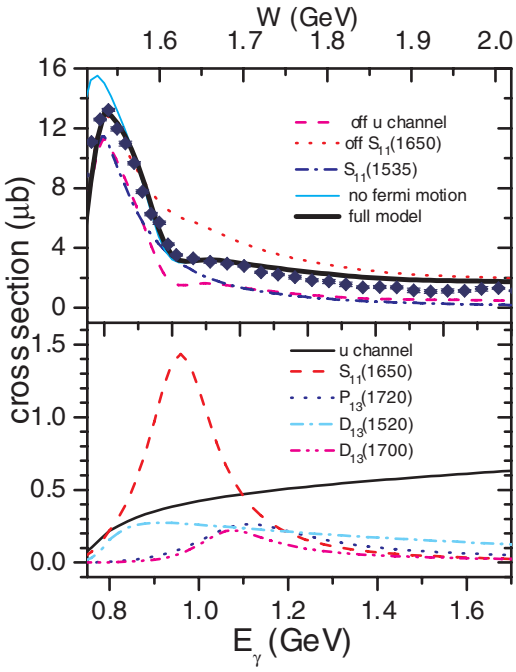

FIG. 5. (Color online) The quasifree cross section for $\gamma p \to \eta p$. The data are taken from Ref. [5]. In the upper panel the bold solid curve corresponds to the full-model result, while the dashed and dotted curves are for the results by switching off the contributions from the u channel and $S_{11}(1650)$, respectively. The partial cross sections for $S_{11}(1535)$, $S_{11}(1650)$, $D_{13}(1520)$, $D_{13}(1700)$, $P_{13}(1720)$, and the u channel are indicated explicitly by the legends in the figures.

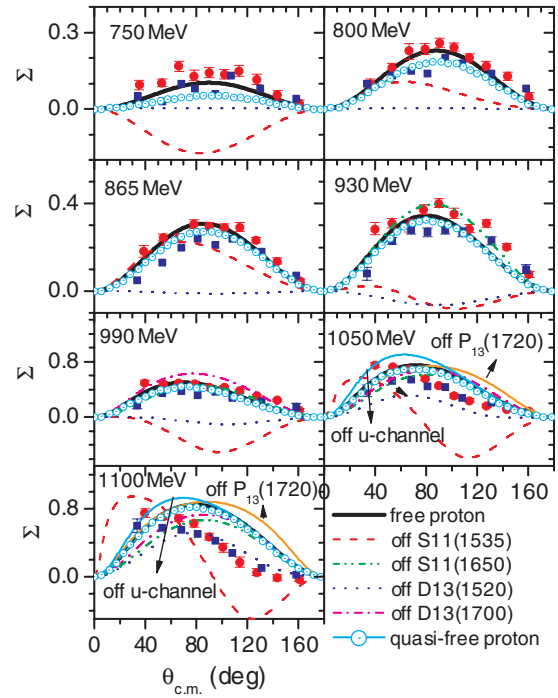

FIG. 6. (Color online) Beam asymmetry Σ in the η photoproduction off quasifree protons as a function of $\theta_{\text{c.m.}}$. The solid squares correspond to the quasifree proton data from Ref. [4], while the solid circles stand for the free proton data from Ref. [46]. The bold solid curves are the full-model results. The results by switching off the contributions from $S_{11}(1535)$, $S_{11}(1650)$, $D_{13}(1520)$, $D_{13}(1700)$, $P_{13}(1720)$, and the u channel are indicated explicitly by the legend.

of no Fermi motion (i.e., the cross section for the free proton reaction in Fig. 3). It shows that the Fermi motion has the most significant corrections around the $S_{11}(1535)$ energy region and becomes negligible in the higher-energy region.

Apart from the Fermi motion corrections, the main feature of the η photoproduction off quasifree protons is similar to the case of a free proton reaction. In particular, we still see the dominance of $S_{11}(1535)$ near threshold and its destructive interference with $S_{11}(1650)$, which accounts for a shallow dip near $E_\gamma \simeq 1.05$ GeV ($W \simeq 1.68$ GeV).

Polarization observables should be more sensitive to the underlying mechanisms. In Fig. 6, we plot the polarized beam asymmetry for $\gamma p \to \eta p$ in comparison with the data for both quasifree (solid circles) and free (open circles) proton reactions. These two sets of data exhibit similarities with each other, which indicate the small effects from the Fermi motion corrections. The theoretical results are able to reproduce the data agreeably up to $E_\gamma \simeq 1.1$ GeV. The discrepancies come up in the higher-energy region of $E_\gamma > 1.05$ GeV, where the contributions from higher resonances may become important.

By switching off the single resonance contributions, we can examine their roles in the reaction. It shows that the large asymmetries in the intermediate angle is due to the dominant S-wave interferences with the D wave.

The interferences of $S_{11}(1535)$ with $D_{13}(1520)$ dominate the beam asymmetry. As shown by the dashed and dotted curves, if we switch off the contributions of $S_{11}(1535)$ and $D_{13}(1520)$, respectively, the asymmetries change drastically. The important roles of $S_{11}(1535)$ and $D_{13}(1520)$ in the beam asymmetry are also suggested in Refs. [30,31,57,58].

The contributions of $S_{11}(1650)$, $D_{13}(1700)$, $P_{13}(1720)$, and the u-channel backgrounds begin to appear in the energy region $E_\gamma > 1.0$ GeV. With the increasing energy the contributions become more and more obvious. $P_{13}(1720)$ seems to be responsible for the shifting of the maximum to forward angles. If we switch off its contributions, the beam asymmetry will keep an approximate forward-backward symmetry.

In brief, it shows that the configuration mixing effects are important for describing $\gamma p \to \eta p$ near threshold. The $S_{11}(1535)$ dominates the cross section, and its destructive interference with the $S_{11}(1650)$ naturally accounts for the dip structure around $W \simeq 1.68$ GeV in the total cross section. The D-wave state [i.e., $D_{13}(1520)$], is crucial for accounting for the angular distributions in the differential cross sections and beam asymmetry, as found by other analyses [15,57–60]. Signals for $D_{13}(1700)$, $P_{13}(1720)$, and the u-channel contributions are also evidential.

D. $\gamma n \to \eta n$ with quasifree neutron target

For the $\gamma n \to \eta n$ process, the Moorhouse selection rule no longer applies. Thus, both the spin-3/2 and spin-1/2 resonances would contribute in the s channel. Apart from the inevitable Fermi motion corrections, another feature with

$\gamma n \to \eta n$ is that the EM interaction only involves neutral hadrons. Therefore, the electric terms would vanish and the leading EM coupling would come from the magnetic terms. As a consequence, the neutron reaction does not share the same resonance strength parameters C_R with the proton reaction, although the strong interaction vertices can be well connected with each other by the isospin symmetry relation. With the same mixing scheme in Eq. (29) we can extract the configuration mixing coefficients for the $S_{11}(1535)$ and $S_{11}(1650)$, which are

$$C^{[70,^2 8]}_{S_{11}(1535)} = R_2^S \cos\theta_S(\cos\theta_S + \sin\theta_S), \quad (33)$$

$$C^{[70,^4 8]}_{S_{11}(1535)} = R_4^S \sin\theta_S(\sin\theta_S + \cos\theta_S), \quad (34)$$

$$C^{[70,^2 8]}_{S_{11}(1650)} = R_2^S \sin\theta_S(\sin\theta_S - \cos\theta_S), \quad (35)$$

$$C^{[70,^4 8]}_{S_{11}(1650)} = R_4^S \cos\theta_S(\cos\theta_S - \sin\theta_S), \quad (36)$$

where R_2^S and R_4^S are introduced to adjust the strength of the partial-wave amplitudes of $[70,^2 8, 1/2^-]$ and $[70,^4 8, 1/2^-]$, respectively, which may be overestimated or underestimated in the naive quark model.

Furthermore, considering the configuration mixing effects in $D_{13}(1520)$ and $D_{13}(1700)$, we extract the configuration mixing coefficient as follows:

$$C^{[70,^2 8]}_{D_{13}(1520)} = R_2^D \cos\theta_D\left(\cos\theta_D - \frac{1}{\sqrt{10}}\sin\theta_D\right), \quad (37)$$

$$C^{[70,^4 8]}_{D_{13}(1520)} = R_4^D \sin\theta_D(\sin\theta_D - \sqrt{10}\cos\theta_D), \quad (38)$$

$$C^{[70,^2 8]}_{D_{13}(1700)} = R_2^D \sin\theta_D\left(\sin\theta_D + \frac{1}{\sqrt{10}}\cos\theta_D\right), \quad (39)$$

$$C^{[70,^4 8]}_{D_{13}(1700)} = R_4^D \cos\theta_D(\cos\theta_D + \sqrt{10}\sin\theta_D), \quad (40)$$

where R_2^D and R_4^D are the constants which are introduced to adjust the strength of the partial-wave amplitudes of $[70,^2 8, 3/2^-]$ and $[70,^4 8, 3/2^-]$, respectively.

In this reaction the mixing angles $\theta_S = 25^\circ$ and $\theta_D = 20^\circ$ are fixed in the $\gamma p \to \eta p$ process. The R values (R_2^S, R_4^S, R_2^D, and R_4^D) and C_R values for the D_{15} and P_{13} resonances are determined by fitting the 90 data points of differential cross sections in the energy region 0.8 GeV $\leqslant E_\gamma \leqslant$ 1.4 GeV with $\chi^2/N = 1.6$. With these fit values, $R_2^S = 0.71$, $R_4^S = 2.95$, $R_2^D = 1.55$, and $R_4^D = 1.0$, we obtain a good description of the differential cross sections, beam asymmetries, and total cross section from threshold up to $E_\gamma \simeq 1.2$ GeV, as shown in Figs. 7–10. With these determined R values, the C_R values for the S and D wave resonances are extracted and listed in Table I.

In $\gamma p \to \eta p$ the main resonance contributions are from $S_{11}(1535)$, $S_{11}(1650)$, $D_{13}(1520)$, $D_{15}(1675)$, and $P_{13}(1720)$. As shown in Table III, the χ^2/N value would increase drastically if any one of these resonances is absent in the fitting. Among the main contributors, the $S_{11}(1535)$ plays a dominant role, as is well-known from the literature. If we turn off its contribution (see the thin solid line in Fig. 7), the differential cross sections become tiny, and the χ^2/N increases to a very large value of 120. The constructive interferences between $S_{11}(1650)$ and $S_{11}(1535)$ around

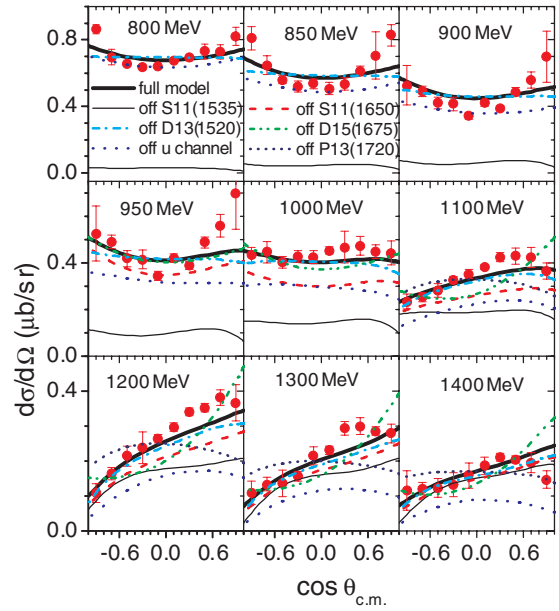

FIG. 7. (Color online) Differential cross sections for the η photoproduction off the quasifree neutron at various beam energies. The data are taken from Ref. [5]. The solid curves correspond to the full-model results. The thin solid, dashed, dash-dotted, dash-dot-dotted, short dashed, and dotted curves are for the results by switching off the contributions from $S_{11}(1535)$, $S_{11}(1650)$, $D_{13}(1520)$, $D_{15}(1675)$, $P_{13}(1720)$, and the u channel, respectively.

$E_\gamma \simeq (1.1 \pm 0.2)$ GeV can be clearly seen in both differential and total cross sections. Turning off the contributions of $S_{11}(1650)$ (see the dashed curves the Fig. 7) the cross section is apparently underestimated. With the constructive interferences between $S_{11}(1535)$ and $S_{11}(1650)$, we can naturally explain the second small bump-like structure at $W \simeq 1.68$ GeV

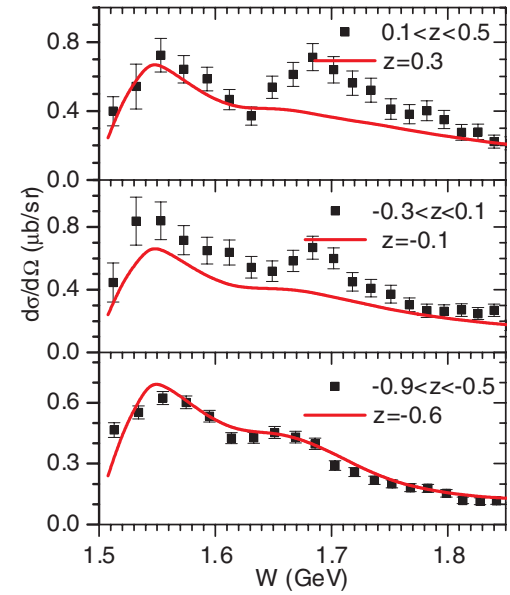

FIG. 8. (Color online) Fixed-angle excitation functions as a function of center mass energy W for the quasifree $\gamma n \to \eta n$ process. Where z is defined by $z = \cos\theta_{\text{c.m.}}$. The data are taken from Ref. [12].

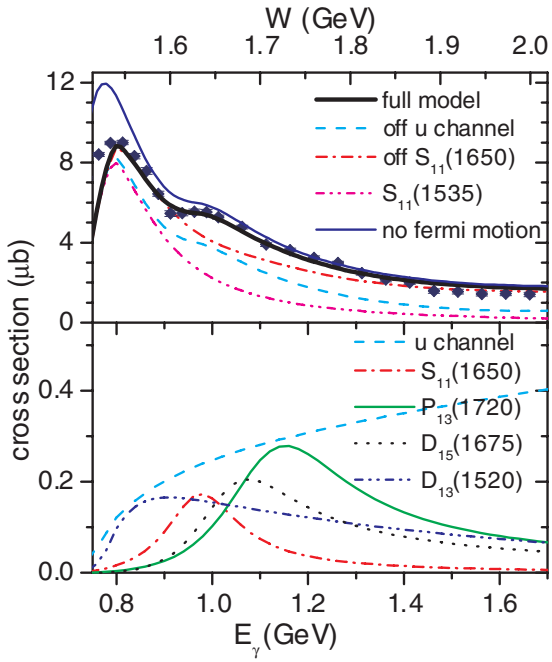

FIG. 9. (Color online) Cross section for the quasifree $\gamma n \to \eta n$ reaction. The data are from Ref. [5]. In the upper panel the heavy (thin) solid curve corresponds to the full model result with (without) Fermi motion corrections, while the dashed and dash-dotted curves are for the results by switching off the contributions from the u channel and $S_{11}(1650)$, respectively. The partial cross sections for $S_{11}(1535)$, $S_{11}(1650)$, $D_{13}(1520)$, $D_{15}(1675)$, $P_{13}(1720)$, and the u channel are indicated explicitly by the legends in the figures.

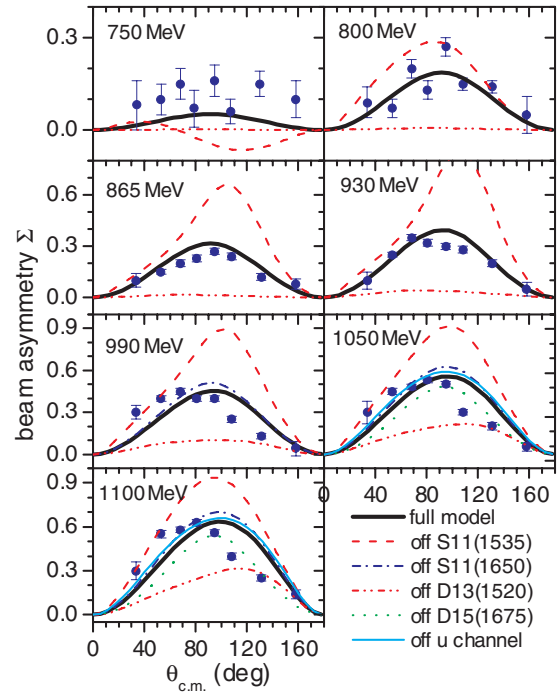

FIG. 10. (Color online) Beam asymmetry Σ in η photoproduction off the quasifree neutron as a function of $\theta_{\text{c.m.}}$. The data are taken from Ref. [4]. The solid curves are the full model results. The results by switching off the contributions from $S_{11}(1535)$, $S_{11}(1650)$, $D_{13}(1520)$, $D_{15}(1675)$, and the u channel are indicated explicitly by the legend in the figure.

($E_\gamma \simeq 1.0$ GeV) in the total cross section and excitation function (see Figs. 8 and 9), although the theoretical results has slightly underestimated the data for the excitation functions at forward angles. Our conclusion is compatible with the recent partial-wave analysis results [14] and the coupled-channel K-matrix approach [15]. The dash-dotted line in the upper panel of Fig. 8 shows that the second bump disappears as long as $S_{11}(1650)$ is switches off. Furthermore, we noted that there are other explanations about the bump-like structure at $W \simeq 1.68$ GeV. For example, Shklyar *et al.* explained the bump-like structure in terms of coupled-channel effects due to $S_{11}(1650)$ and $P_{11}(1710)$ [16]. In Refs. [10,11], the structure around $W = 1.68$ GeV was even considered as evidence for a nonstrange member of the antidecuplet pentaquark state $P_{11}(1670)$ [61].

$D_{13}(1520)$ is crucial for the shape change of the differential cross sections in the low-energy region $E_\gamma < 1.0$ GeV, although its effects on the total cross section are negligible. The dash-dotted curves in Fig. 7 show that, without its contributions, the forward angle enhancement would disappear. The importance of $D_{13}(1520)$ can also be seen in the beam asymmetry. In Fig. 10 it shows that the interferences between $D_{13}(1520)$ and $S_{11}(1535)$ govern the beam asymmetry in the low-energy region $E_\gamma < 1.1$ GeV. Switching off the $D_{13}(1520)$ (dash-dot-dotted curves) or $S_{11}(1535)$ (dashed curves), we find that the curves change drastically.

A relatively large contribution from the $D_{15}(1675)$ with $C_{D_{15}(1675)} = 1.8$ seems to be favored by the experimental data. In Fig. 7, as indicated by the dash-dot-dotted lines, the cross sections at forward angles are overestimated significantly without the $D_{15}(1675)$. The relatively large strength parameter $C_{D_{15}(1675)} = 1.8$ for the $D_{15}(1675)$ might due to the underestimate of the helicity couplings in the naive quark model. In the SU(6)⊗O(3) symmetry limit, the helicity couplings of $D_{15}(1675)$ are $A^n_{1/2} \simeq -0.032$ GeV$^{-1/2}$ and $A^n_{3/2} \simeq -0.045$ GeV$^{-1/2}$, which are much smaller than the center values from the PDG [45].

In the SU(6)⊗O(3) symmetry limit, the contributions of $P_{13}(1720)$ are too small to reproduce the forward peak in the differential cross sections in the energy region $E_\gamma \simeq (1.2 \pm 0.1)$ GeV. By fitting the data, it shows that a relatively large value $C_{P_{13}(1720)} = 3.0$ should be applied. As denoted by the short-dashed line in Fig. 7 we see that, without $P_{13}(1720)$, the forward peak in the differential cross sections would disappear. Contributions from $P_{13}(1720)$ were also suggested by Klempt *et al.* [14]. The unexpectedly large strength parameter of $P_{13}(1720)$ in the reaction could be an indication that SU(6)⊗O(3) symmetry is badly violated [62].

The u-channel background also plays an important role in the $\gamma n \to \eta n$ process. It has a constructive interferences with $S_{11}(1535)$. As shown by the dotted lines in Fig. 7 and the dashed line in the upper panel of Fig. 9, the cross sections will be underestimated more and more obviously with increasing energy if the u channel is switched off.

In the lower panel of the Fig. 9, it shows that $D_{13}(1520)$, $D_{15}(1675)$, $P_{13}(1720)$, and the background u channel have comparable exclusive cross sections with $S_{11}(1650)$ around $E_\gamma \simeq 1.1$ GeV. Their overall interfering effects have been essential for a good description of the experimental observable in this energy region. For instance, it can be noticed that the angular distributions of the cross sections are sensitive to $D_{13}(1520)$, $D_{15}(1675)$, and $P_{13}(1720)$, although their effects on the total cross section are negligible. Furthermore, $S_{11}(1650)$, $D_{15}(1675)$, and the background u channel have also sizable effects on beam asymmetry. Comparing with the data, we find that the predicted maximum for the beam asymmetry slightly shifts to the backward angles in the region $E_\gamma \gtrsim 1.0$ GeV. It might indicate that higher resonances have interferences and they should be included with more elaborate considerations.

We also mention that other resonances, such as $P_{11}(1440)$, $P_{11}(1710)$, and $D_{13}(1700)$, have negligible effects in the η photoproduction.

Similar to the $\gamma p \to \eta p$ process with quasifree protons, the Fermi motion brings corrections to the cross section from threshold up to the mass of $S_{11}(1535)$. The effects decrease with increasing energy, as denoted by the thin solid curve in the upper panel of Fig. 9.

To briefly summarize this subsection, we show that, with the well-established $S_{11}(1535)$, $S_{11}(1650)$, $D_{13}(1520)$, $D_{15}(1675)$, and $P_{13}(1720)$ resonances and contribution of the u channel, we obtained a good description of the reaction $\gamma n \to \eta n$ with quasifree neutrons. In this reaction, $S_{11}(1535)$ plays a dominated role similar to $\gamma p \to \eta p$. However, due to the presence of [70,[4] 8] states, the amplitude of $S_{11}(1535)$ appears to have a constructive interference with $S_{11}(1650)$, which is crucial to explain the bump-like structure around $W = 1.68$ GeV. We also find that the angular distributions of the differential cross sections are sensitive to $D_{15}(1675)$ and $P_{13}(1720)$ around $E_\gamma = 1.1$ GeV, and the u channel contributes a large background to the differential cross sections. The interferences between $D_{13}(1520)$ and $S_{11}(1535)$ govern the beam asymmetry at the low-energy region $E_\gamma < 1.1$ GeV, while contributions of several other resonances, such as $P_{11}(1440)$, $P_{11}(1710)$, and $D_{13}(1700)$, are negligibly small.

E. σ_n/σ_p with quasifree neutron target

With the reasonable description of the η photoproduction off the free nucleons available, we can proceed a prediction for the quasifree neutron-to-proton cross-section ratio, σ_n/σ_p. This quantity was measured by the CBELSA/TAPS Collaboration [5]. In Fig. 11 the theoretical prediction is plotted as the solid curve to compare with the experimental measurement [5]. It shows that the data can be well described by the solid curve, and an enhancement around $W \simeq 1.68$ GeV is observable.

In the literature this sharp peak at $W \simeq 1.68$ GeV is considered as evidence of a new resonance [3,6–8,10–12]. However, in our case it can be naturally interpreted as the interferences between $S_{11}(1650)$ and $S_{11}(1535)$ (i.e., destructive in $\gamma p \to \eta p$ but constructive in $\gamma n \to \eta n$). The dashed curve in Fig. 11 denotes the cross-section ratio with $S_{11}(1650)$ switched off. It shows that the ratio becomes flat and that the sharp peak disappears. Our prediction agrees with that of the recent partial-wave analysis [14]. The ratio is also studied within a unitary coupled-channel model; it is interpreted by the coupled-channel effect in S waves, where the $S_{11}(1535)$ is dynamically generated [39].

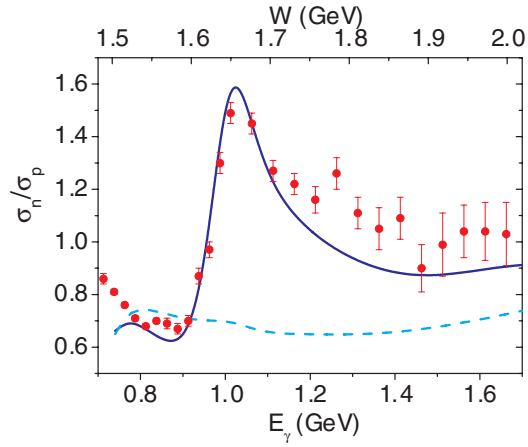

FIG. 11. (Color online) Cross-section ratio σ_n/σ_p for the quasifree reactions $\gamma n \to \eta n$ and $\gamma p \to \eta p$ as a function of photon energy. The data are taken from Ref. [5]. The dashed curve is the result with $S_{11}(1650)$ switched off.

F. Helicity amplitudes

The helicity amplitudes of the nucleon resonances can be extracted by the relation [63],

$$A^{n,p}_{1/2,3/2} = \sqrt{\frac{|\mathbf{q}|M_R\Gamma_R}{|\mathbf{k}|M_N b_\eta}}\,\xi^{n,p}_{1/2,3/2}, \tag{41}$$

where $b_\eta \equiv \Gamma_{\eta N}/\Gamma_R$ is the branching ratio of the resonance, which can be obtained from the experimental determinations. The quantity ξ for different resonances can be analytically expressed from their CGLN amplitudes. In this work, we have given the expressions for ξ for the low-lying S- and D-wave resonances in Table IV.

In the calculations we take the branching ratios of various resonances from Refs. [45,58,59,64], which have been listed in Table V. Together with the model parameter fixed, we can extract the helicity amplitudes of those low-lying S- and D-wave resonances that are listed in Table V. The PDG values [45] are also listed as a comparison. It is found that the predicted magnitudes for $A_{1/2}$ and $A_{3/2}$ are compatible with the PDG values at the 30% level.

It should be mentioned that when we take the small branching ratio $b_\eta = 0.05 \pm 0.02\%$ from Refs. [58,59] for $D_{13}(1520)$, its extracted helicity amplitudes are good agreement with the values from PDG. However, if we use the large branching ratio $b_\eta = 2.3 \pm 0.4\%$ from PDG, the helicity amplitudes are too small to be comparable with the experimental values.

Furthermore, we have noted that the $A^n_{1/2}$ for $S_{11}(1650)$ extracted by us has a positive sign, which is opposite to

TABLE IV. The expressions of ξ in Eq. (41) for various resonances. Where we have defined $\mathcal{K} \equiv [\alpha_e \alpha_\eta \pi (M_N + E_f)/M_R^3]^{1/2}/\Gamma_R$, $\mathcal{A} \equiv [\frac{2\omega_\gamma}{m_q} - \frac{2q^2}{3\alpha^2}(1 + \frac{\omega_\eta}{E_f + M_N})] \exp[-(k^2+q^2)/(6\alpha^2)]$, and $\mathcal{B} = -\frac{2q^2}{3\alpha^2}(1 + \frac{\omega_\eta}{E_f + M_N}) \exp[-(k^2+q^2)/(6\alpha^2)]$.

Resonance	ξ	Expression
$S_{11}(1535)$	$\xi^p_{1/2}$	$\mathcal{K}\frac{\omega_\gamma}{6}(1 + \frac{\omega_\gamma}{2m_q})\mathcal{A}C^{[70,^2 8]p}_{S_{11}(1535)}$
	$\xi^n_{1/2}$	$-\mathcal{K}[\frac{\omega_\gamma}{6}(1 + \frac{\omega_\gamma}{6m_q})C^{[70,^2 8]n}_{S_{11}(1535)} + \frac{\omega_\gamma^2}{36m_q}C^{[70,^4 8]n}_{S_{11}(1535)}]\mathcal{A}$
$S_{11}(1650)$	$\xi^p_{1/2}$	$-\mathcal{K}\frac{\omega_\gamma}{6}(1 + \frac{\omega_\gamma}{2m_q})\mathcal{A}C^{[70,^2 8]p}_{S_{11}(1650)}$
	$\xi^n_{1/2}$	$\mathcal{K}[\frac{\omega_\gamma}{6}(1 + \frac{\omega_\gamma}{6m_q})C^{[70,^2 8]n}_{S_{11}(1650)} + \frac{\omega_\gamma^2}{36m_q}C^{[70,^4 8]n}_{S_{11}(1650)}]\mathcal{A}$
$D_{13}(1520)$	$\xi^p_{1/2}$	$-\mathcal{K}\sqrt{\frac{1}{2}}\frac{\omega_\gamma}{6}(1 - \frac{\omega_\gamma}{m_q})\mathcal{B}C^{[70,^2 8]p}_{D_{13}(1520)}$
	$\xi^p_{3/2}$	$\mathcal{K}\sqrt{\frac{1}{2}}\frac{\omega_\gamma}{6}\mathcal{B}C^{[70,^2 8]p}_{D_{13}(1520)}$
	$\xi^n_{1/2}$	$-\sqrt{\frac{1}{2}}\mathcal{K}[\frac{\omega_\gamma}{6}(1 - \frac{\omega_\gamma}{3m_q})C^{[70,^2 8]n}_{D_{13}(1520)} + \frac{\omega_\gamma^2}{180m_q}C^{[70,^4 8]n}_{D_{13}(1520)}]\mathcal{B}$
	$\xi^n_{3/2}$	$-\sqrt{\frac{1}{2}}\mathcal{K}[\frac{\omega_\gamma}{2\sqrt{3}}C^{[70,^2 8]n}_{D_{13}(1520)} + \frac{\omega_\gamma^2}{20\sqrt{3}m_q}C^{[70,^4 8]n}_{D_{13}(1520)}]\mathcal{B}$
$D_{13}(1700)$	$\xi^n_{1/2}$	$-\sqrt{\frac{1}{2}}\mathcal{K}[\frac{\omega_\gamma}{6}(1 - \frac{\omega_\gamma}{3m_q})C^{[70,^2 8]n}_{D_{13}(1700)} + \frac{\omega_\gamma^2}{180m_q}C^{[70,^4 8]n}_{D_{13}(1700)}]\mathcal{B}$
	$\xi^n_{3/2}$	$-\sqrt{\frac{1}{2}}\mathcal{K}[\frac{\omega_\gamma}{2\sqrt{3}}C^{[70,^2 8]n}_{D_{13}(1700)} + \frac{\omega_\gamma^2}{20\sqrt{3}m_q}C^{[70,^4 8]n}_{D_{13}(1700)}]\mathcal{B}$
	$\xi^p_{1/2}$	$-\mathcal{K}\sqrt{\frac{1}{2}}\frac{\omega_\gamma}{6}(1 - \frac{\omega_\gamma}{m_q})\mathcal{B}C^{[70,^2 8]p}_{D_{13}(1700)}$
	$\xi^p_{3/2}$	$\mathcal{K}\sqrt{\frac{1}{2}}\frac{\omega_\gamma}{6}\mathcal{B}C^{[70,^2 8]p}_{D_{13}(1700)}$
$D_{15}(1675)$	$\xi^n_{1/2}$	$-\mathcal{K}\frac{\omega_\gamma^2}{40m_q}\mathcal{B}C_{D_{15}(1675)}$
	$\xi^n_{3/2}$	$-\mathcal{K}\frac{\omega_\gamma^2}{20\sqrt{2}m_q}\mathcal{B}C_{D_{15}(1675)}$

that of other predictions [14,51,65–67]. Without configuration mixing between $[70,^2 8]$ and $[70,^4 8]$, the value of $A^n_{1/2}$ for $S_{11}(1650)$ predicted from the quark model is positive, which comes totally from $[70,^4 8]$ [51,65–67]. However, when the configuration mixing effects are included, the previous quark-model study predicted a negative value of $A^n_{1/2}$ for $S_{11}(1650)$, which is dominated by $[70,^2 8]$ [51,65–67]. In this work, we make some corrections for the amplitudes of $[70,^2 8]$ and $[70,^4 8]$ to reproduce the data for $\gamma n \to \eta n$ reaction. It is found that a strong contribution of $[70,^4 8]$ might be needed in the reaction, which leads to a dominant contribution of $[70,^4 8]$ to the $A^n_{1/2}$ in the configuration mixing scheme. Thus, we obtain a positive sign.

The branching ratio b_η for $D_{15}(1675)$ has a large uncertainty. With the upper limit of b_η (i.e., $b_\eta = 0.01$), the extracted helicity amplitudes $A^n_{1/2} \simeq -40$ and $A^n_{1/2} \simeq -56$ are in good agreement with the values of PDG, which indicates that the branching ratio b_η might favor a large value of $b_\eta \simeq 0.01$.

IV. SUMMARY

In this work, we have studied the η photoproduction off the quasifree nucleons within a chiral quark model. Our main motivation is to study the bump-like structure observed in the ηn process around $W \simeq 1.68$ GeV. We have achieved good descriptions of the differential cross sections, total cross sections, and polarized beam asymmetries for both processes in the three-quark scenario for the baryon resonances.

It is found that the constructive interference between $S_{11}(1650)$ and $S_{11}(1535)$ is responsible for the bump-like structure around $W \simeq 1.68$ GeV in the $\gamma n \to \eta n$ process,

TABLE V. Estimated helicity amplitudes of the S- and D-wave resonances (in 10^{-3} GeV$^{-1/2}$).

Resonance	$A^p_{1/2}$	$A^p_{1/2}$(PDG)	$A^p_{3/2}$	$A^p_{3/2}$(PDG)	$A^n_{1/2}$	$A^n_{1/2}$(PDG)	$A^n_{3/2}$	$A^n_{3/2}$ (PDG)	b_η used in this work
$S_{11}(1535)$	60 ± 5	90 ± 30			-68 ± 5	-46 ± 27			$0.45 \sim 0.60$ [45]
$S_{11}(1650)$	41 ± 13	53 ± 16			24 ± 7	-15 ± 21			$3 \sim 10\%$ [45]
$D_{13}(1520)$	-32 ± 7	-24 ± 9	113 ± 23	166 ± 5	-40 ± 8	-59 ± 9	-124 ± 26	-139 ± 11	$0.05 \pm 0.02\%$ [58,59]
$D_{13}(1700)$	-12 ± 4	-18 ± 13	24 ± 8	-2 ± 24	-2 ± 1	0 ± 50	-3 ± 1	-3 ± 44	0.1 ± 0.06 [64]
$D_{15}(1675)$		19 ± 8		15 ± 9	-40^a	-43 ± 12	-56^a	-58 ± 13	0.0 ± 0.01 [45]

[a]These helicity amplitudes of $D_{15}(1675)$ are obtained with $b_\eta = 0.01$.

while the destructive interference between $S_{11}(1650)$ and $S_{11}(1535)$ produces the shallow dip around $W \simeq 1.68$ GeV in the total cross section of $\gamma p \to \eta p$. Such interferences can lead to a sharp peak in the ratio of σ_n/σ_p at $W \simeq 1.68$ GeV. We also find that no new resonances are needed for both of the processes to interpret the observations in a rather broad energy region above the threshold. We note that the importance of the interference between $S_{11}(1650)$ and $S_{11}(1535)$ are also found for the $\pi p \to \eta n$ process in our previous studies [68].

Apart from $S_{11}(1535)$ and $S_{11}(1650)$, $D_{13}(1520)$ also plays an important role in both of the reactions. It accounts for the major deviations of the angular distributions of the cross section from an S wave and also produces large beam asymmetries near threshold. The u-channel background cannot be neglected for both of the processes. It enhances the cross sections obviously. Our calculation favors a much larger contribution from $P_{13}(1720)$ around its threshold. Since it is within the second orbital excitation multiplets, such an enhanced strength could imply the breakdown of SU(6)⊗O(3) symmetry. Furthermore, elaborate treatment for higher-excited states should be considered. We also find that, around $W \simeq 1.7$ GeV, $D_{15}(1675)$ is crucial for the angular distributions of the cross section for $\gamma n \to \eta n$, while $D_{13}(1700)$ plays an important role in $\gamma p \to \eta p$.

It should be emphasized that the configuration mixing effects in the S- and D-wave resonances are important for describing $\gamma p \to \eta p$ near threshold. We have estimated the mixing angles θ_S and θ_D, which are $\theta_S \simeq 26^\circ$ and $\theta_D \simeq 21^\circ$. These mixings are also included in $\gamma n \to \eta n$, although some ambiguities would arise from the EM couplings. A more detailed study of this issue will be reported elsewhere.

In this work, we have extracted the helicity amplitudes for the S- and D-wave resonances $S_{11}(1535)$, $S_{11}(1650)$, $D_{13}(1520)$, $D_{13}(1700)$, and $D_{15}(1675)$ from the reactions, which are compatible with the values from the PDG.

ACKNOWLEDGMENTS

This work is supported in part by the National Natural Science Foundation of China (Grant Nos. 10775145, 11075051, and 11035006), Chinese Academy of Sciences (KJCX2-EW-N01), Program for Changjiang Scholars and Innovative Research Team in University (PCSIRT, No. IRT0964), Ministry of Science and Technology of China (2009CB825200), the Program Excellent Talent Hunan Normal University, and the Hunan Provincial Natural Science Foundation (11JJ7001).

[1] E. Klempt and J. M. Richard, Rev. Mod. Phys. **82**, 1095 (2010).
[2] B. Krusche and S. Schadmand, Prog. Part. Nucl. Phys. **51**, 399 (2003).
[3] GRAAL Collaboration, V. Kuznetsov, *Proceedings of Workshop on the Physics of Excited Nucleons (NSTAR 2004), Grenoble, France*.
[4] A. Fantini *et al.*, Phys. Rev. C **78**, 015203 (2008).
[5] CBELSA Collaboration and TAPS Collaboration, I. Jaegle *et al.*, Phys. Rev. Lett. **100**, 252002 (2008).
[6] F. Miyahara *et al.*, Prog. Theor. Phys. Suppl. **168**, 90 (2007).
[7] Crystal Ball Collaboration and TAPS Collaboration, D. Werthmuller, Chin. Phys. C **33**, 1345 (2009).
[8] V. Kuznetsov *et al.*, Phys. Rev. C **83**, 022201 (2011).
[9] Y. I. Azimov, V. Kuznetsov, M. V. Polyakov, and I. Strakovsky, Eur. Phys. J. A **25**, 325 (2005).
[10] A. Fix, L. Tiator, and M. V. Polyakov, Eur. Phys. J. A **32**, 311 (2007).
[11] K. S. Choi, S. i. Nam, A. Hosaka, and H. C. Kim, Phys. Lett. B **636**, 253 (2006).
[12] GRAAL Collaboration, V. Kuznetsov *et al.*, Phys. Lett. B **647**, 23 (2007).
[13] V. Kuznetsov, M. V. Polyakov, and M. Thurmann, JETP Lett. **94**, 543 (2011).
[14] A. V. Anisovich, I. Jaegle, E. Klempt, B. Krusche, V. A. Nikonov, A. V. Sarantsev, and U. Thoma, Eur. Phys. J. A **41**, 13 (2009).
[15] R. Shyam and O. Scholten, Phys. Rev. C **78**, 065201 (2008).
[16] V. Shklyar, H. Lenske, and U. Mosel, Phys. Lett. B **650**, 172 (2007).
[17] V. Kuznetsov, M. Polyakov, T. Boiko, J. Jang, A. Kim, W. Kim, and A. Ni, arXiv:hep-ex/0703003.
[18] Crystal Ball Collaboration, E. F. McNicoll *et al.*, Phys. Rev. C **82**, 035208 (2010).
[19] T. Abdullah and F. E. Close, Phys. Rev. D **5**, 2332 (1972).
[20] F. E. Close and Z. P. Li, Phys. Rev. D **42**, 2194 (1990).
[21] Z. P. Li, Phys. Rev. D **48**, 3070 (1993); **50**, 5639 (1994); Phys. Rev. C **52**, 1648 (1995).
[22] Z. P. Li, H. X. Ye, and M. H. Lu, Phys. Rev. C **56**, 1099 (1997).
[23] Q. Zhao, J. S. Al-Khalili, and C. Bennhold, Phys. Rev. C **64**, 052201 (2001).
[24] Q. Zhao, J. S. Al-Khalili, Z. P. Li, and R. L. Workman, Phys. Rev. C **65**, 065204 (2002).
[25] Q. Zhao, B. Saghai, and Z. P. Li, J. Phys. G **28**, 1293 (2002).
[26] Q. Zhao, Z. P. Li, and C. Bennhold, Phys. Rev. C **58**, 2393 (1998); Phys. Lett. B **436**, 42 (1998).
[27] Z. P. Li, Phys. Rev. D **52**, 4961 (1995).
[28] Z. P. Li and B. Saghai, Nucl. Phys. A **644**, 345 (1998).
[29] B. Saghai and Z. p. Li, Eur. Phys. J. A **11**, 217 (2001).
[30] J. He, B. Saghai, and Z. Li, Phys. Rev. C **78**, 035204 (2008).
[31] J. He and B. Saghai, Phys. Rev. C **80**, 015207 (2009).
[32] R. G. Moorhouse, Phys. Rev. Lett. **16**, 772 (1966).
[33] N. Isgur and G. Karl, Phys. Rev. D **18**, 4187 (1978).
[34] N. Isgur and G. Karl, Phys. Lett. B **72**, 109 (1977).
[35] R. Dolen, D. Horn, and C. Schmid, Phys. Rev. **166**, 1768 (1968).
[36] J. He, B. Saghai, Z. Li, Q. Zhao, and J. Durand, Eur. Phys. J. A **35**, 321 (2008).
[37] G. F. Chew, M. L. Goldberger, F. E. Low, and Y. Nambu, Phys. Rev. **106**, 1345 (1957).
[38] R. L. Walker, Phys. Rev. **182**, 1729 (1969).
[39] M. Doring and K. Nakayama, Phys. Lett. B **683**, 145 (2010).
[40] M. Lacombe, B. Loiseau, R. Vinh Mau, J. Cote, P. Pires, and R. de Tourreil, Phys. Lett. B **101**, 139 (1981).
[41] R. Machleidt, Phys. Rev. C **63**, 024001 (2001).
[42] L. Tiator, C. Bennhold, and S. S. Kamalov, Nucl. Phys. A **580**, 455 (1994).
[43] J. Piekarewicz, Phys. Rev. C **48**, 1555 (1993).
[44] S. L. Zhu, Phys. Rev. C **61**, 065205 (2000).
[45] C. Amsler *et al.*, Phys. Lett. B **667**, 1 (2008).

[46] GRAAL Collaboration, O. Bartalini *et al*., Eur. Phys. J. A **33**, 169 (2007).
[47] CB-ELSA Collaboration, V. Crede *et al*., Phys. Rev. Lett. **94**, 012004 (2005).
[48] X.-H. Liu, X.-H. Zhong, and Q. Zhao (unpublished).
[49] B. Saghai and Z. Li, Few-Body Syst. **47**, 105 (2010).
[50] C. An and B. Saghai, arXiv:1108.3282.
[51] R. Koniuk and N. Isgur, Phys. Rev. D **21**, 1868 (1980); **23**, 818 (1981).
[52] J. Chizma and G. Karl, Phys. Rev. D **68**, 054007 (2003).
[53] D. Pirjol and C. Schat, Phys. Rev. D **67**, 096009 (2003).
[54] S. Capstick and W. Roberts, Fizika B **13**, 271 (2004).
[55] J. He, B. Saghai, Z. Li, Q. Zhao, and J. Durand, Eur. Phys. J. A **35**, 321 (2008).
[56] K. Nakayama, Y. Oh, H. Haberzettl, and J. Korean, Phys. Soc. **59**, 224 (2011).
[57] W. T. Chiang, S. N. Yang, L. Tiator, M. Vanderhaeghen, and D. Drechsel, Phys. Rev. C **68**, 045202 (2003).
[58] L. Tiator, D. Drechsel, G. Knochlein, and C. Bennhold, Phys. Rev. C **60**, 035210 (1999).
[59] W. T. Chiang, S. N. Yang, L. Tiator, and D. Drechsel, Nucl. Phys. A **700**, 429 (2002).
[60] G. Knochlein, D. Drechsel, and L. Tiator, Z. Phys. A **352**, 327 (1995).
[61] R. L. Jaffe and F. Wilczek, Phys. Rev. Lett. **91**, 232003 (2003).
[62] Q. Zhao and F. E. Close, Phys. Rev. D **74**, 094014 (2006).
[63] M. Benmerrouche, N. C. Mukhopadhyay, and J. F. Zhang, Phys. Rev. D **51**, 3237 (1995).
[64] M. Batinic, I. Slaus, A. Svarc, and B. M. K. Nefkens, Phys. Rev. C **51**, 2310 (1995); **57**, 1004 (1998).
[65] Z. Li and F. E. Close, Phys. Rev. D **42**, 2207 (1990).
[66] R. Bijker, F. Iachello, and A. Leviatan, Annals Phys. **236**, 69 (1994).
[67] S. Capstick, Phys. Rev. D **46**, 2864 (1992).
[68] X. H. Zhong, Q. Zhao, J. He, and B. Saghai, Phys. Rev. C **76**, 065205 (2007).